Available online at www.sciencedirect.com
ScienceDirect
Journal of Power Sources 177 (2008) 96–103
JOURNAL OF POWER SOURCES
www.elsevier.com/locate/jpowsour

Three-dimensional numerical analysis of PEM fuel cells with straight and wave-like gas flow fields channels

Jenn-Kun Kuo [a], Tzu-Hsiang Yen [b], Cha'o-Kuang Chen [b,*]

[a] *Graduate Institute of Greenergy Technology, National University of Tainan, Tainan 70005, Taiwan, ROC*
[b] *Department of Mechanical Engineering, National Cheng Kung University, Tainan 70101, Taiwan, ROC*

Received 6 October 2007; received in revised form 6 November 2007; accepted 7 November 2007
Available online 26 November 2007

Abstract

Using a three-dimensional computational model, numerical simulations are performed to investigate the performance characteristics of proton exchange membrane fuel cells (PEMFCs) incorporating either a conventional straight gas flow channel or a novel wave-like channel. The simulations focus particularly on the effect of the wave-like surface on the gas flow characteristics, the temperature distribution, the electrochemical reaction efficiency and the electrical performance of the PEMFCs at operating temperatures ranging from 323 K to 343 K. The numerical results reveal that the wave-like surface enhances the transport of the reactant gases through the porous layer, improves the convective heat transfer effect, increases the gas flow velocity, and yields a more uniform temperature distribution. As a result, the efficiency of the catalytic reaction is significantly improved. Consequently, compared to a conventional PEMFC, the PEMFC with a wave-like channel yields a notably higher output voltage and power density.

Keywords: Proton exchange membrane (PEM); Wave-like gas flow channel; Temperature; Numerical simulation

1. Introduction

Since their introduction by NASA in the 1960s, proton exchange membrane fuel cells (PEMFCs) have attracted considerable interest within industrial and academic circles as a potential power source for a range of mobile applications. Characterized by a compact size, an efficient performance, a straightforward design and operation, and a high degree of environmental friendliness, it seems likely that PEMFCs will one day replace gasoline and diesel internal combustion engines as the method of choice for vehicular applications. The literature contains many experimental and numerical investigations into the transport phenomena and electrical performance of PEMFCs. For example, Springer et al. [1] developed a one-dimensional isothermal model of a PEMFC and showed that the water diffusion coefficient, electro-osmotic drag coefficient, water sorption isothermals and membrane conductivities all varied as a function of the membrane water content.

In a PEMFC, the design of the flow delivery system has a critical effect on the cell performance. Various flow channel designs have been proposed, including straight, serpentine and inter-digitated. Whilst each configuration has its own particular advantages, the inter-digitated design has attracted particular interest due to its efficiency in expelling the liquid water byproduct from the porous electrode. For example, in [2], two dead-end flow channels were used to force the reactant gases through the diffusion layer via a convection effect rather than diffusion. It was shown that the resultant shear force acting on the fluid prompted the forcible ejection of liquid water from the pores of the membrane. Many sophisticated numerical models have been developed to enable the influence of the flow field configuration on the transport phenomena and electrical performance of a PEMFC to be evaluated [3–6].

In conventional PEMFCs with straight gas flow channels, the reactant gases diffuse into the catalyst layer through the gas diffusion layer. However, the diffusion process is inherently slow, and hence the electrical performance of the PEMFC is inevitably limited. In an attempt to resolve this problem, Kuo and Chen [7–9] proposed a novel PEMFC design in which the gas flow channel had a wave-like structure. Using a 3D computational model, the authors showed that this unique channel design

* Corresponding author. Tel.: +886 6 2757575x62140; fax: +886 6 2342081.
E-mail address: ckchen@mail.ncku.edu.tw (C.-K. Chen).

0378-7753/$ – see front matter © 2007 Published by Elsevier B.V.
doi:10.1016/j.jpowsour.2007.11.065

Nomenclature

C	mass fraction
C_F	quadratic drag factor
D	mass diffusion ($m^2\ s^{-1}$)
F	Faraday's constant (96,485 C mol^{-1})
i_e	current density ($A\ m^{-2}$)
i_m	ionic current density ($A\ m^{-2}$)
j	transfer current density ($A\ m^{-3}$)
k_c	condensation rate constant ($1\ s^{-1}$)
k_e	evaporation rate constant ($1\ (atm\ s)^{-1}$)
k_p	permeability (m^2)
k_m^{eff}	effective ionic conductivity of membrane ($S\ cm^{-1}$)
k_s^{eff}	elective electric conductivity of the GDL ($S\ cm^{-1}$)
M	molecular weight ($kg\ mol^{-1}$)
n	charge number of the sulfonic acid ions
P	pressure (atm)
R	universal gas constant ($8.314\ J\ (mol\ k)^{-1}$)
S	source term
T	Temperature (K)
u	velocity in the x-direction ($m\ s^{-1}$)
v	velocity in the y-direction ($m\ s^{-1}$)
V	operating voltage (V)
w	velocity in the z-direction ($m\ s^{-1}$)
Z_f	species valence

Greek symbols

α	transfer coefficient for the reaction
β	coefficient of thermal expansion
ε	porosity
λ	water content of membrane
ρ	density ($kg\ cm^{-2}$)
σ	ionic conductivity ($1\ (\Omega\ m)^{-1}$)
τ	tortuosity
υ	viscosity of flow ($kg\ (m\ s)^{-1}$)
Φ	phase potential (V)
η_{act}	activation overpotential (V)

Subscripts

a	anode
c	cathode
CL	catalyst layer
e	energy
eff	effective
GDL	gas diffusion layer
h_1	gas flow channel height
h_2	gas diffusion channel height
in	inlet
k	kth component of fuel reactant
m	membrane phase
mem	membrane
out	outlet, outer
ref	reference
w	wall
x	x-direction
y	y-direction
z	z-direction

improved the uniformity of the velocity and temperature distributions within the channel and reduced the intersection angle between the dimensionless velocity vector and the temperature gradient, thereby improving the heat transfer characteristics of the fuel cell.

The current study performs a series of 3D numerical simulations to investigate the influence of the forced convection effect [10,11] induced in the wave-like gas flow channel on the velocity, temperature and gas concentration distributions within the PEMFC. The electrical performance of a PEMFC with a wave-like gas flow channel is then compared with that of a fuel cell with a conventional straight channel at temperatures of 323 K, 333 K and 343 K, respectively. The validity of the numerical model is confirmed by comparing the results obtained for the electrical performance of the PEMFC with a straight channel with the experimental results presented by Wang et al. [12].

2. Simulation model

The simulations performed in this study are based on a steady-state, single-phase, multi-species, three-dimensional mass transfer model of the PEMFC. Fig. 1 presents a 3D schematic illustration of the fuel cell. As shown, the major components include: (1) two wave-like flow channels, (2) two carbon paper gas diffusion layers (GDLs), (3) two catalyst layers and (4) a porous membrane. The geometric and physical parameters applied in the simulations are summarized in Table 1. Note that some minor parameters (e.g. the internal resistance, the material properties, and so forth) are omitted from this table, but can be found in the literatures [13–15]. The operating pressure and temperature are assumed to be 1 atm and 323 K, 333 K or 343 K, respectively. Regarding the reactant gases, the anode is supplied with humidified hydrogen with a mass fraction of

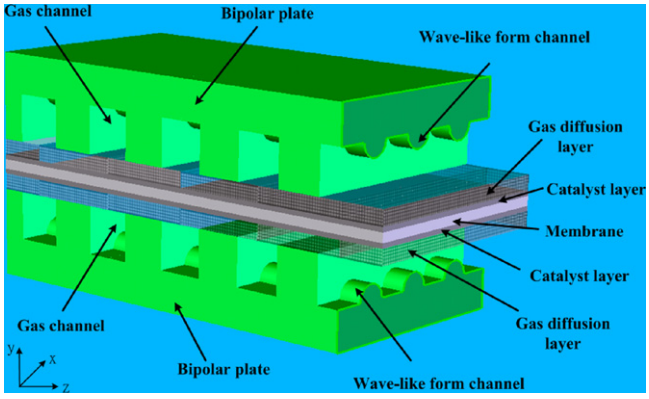

Fig. 1. Schematic representation of PEMFC.

Table 1
Geometric and physical parameters employed in numerical simulations

Quantity	Value
Gas channel depth	0.5 mm
Gas channel width	0.5 mm
Gas channel length	100 mm
Gas diffusion layer thickness	0.3 mm
Catalyst thickness	0.05 mm
Membrane thickness	0.125 mm
Porosity of gas diffusion layer	0.4
Porosity of catalyst layer	0.28
Permeability of gas diffusion layer	1.76×10^{-11} m^2
Permeability of catalyst layer	1.76×10^{-11} m^2
Permeability of membrane layer	1.18×10^{-18} m^2
Tortuosity of gas diffusion layer	1.5
Tortuosity of catalyst layer	1.5
Electronic conductivity of gas diffusion layer	53 S m^{-1}
Electronic conductivity of catalyst layer	53 S m^{-1}
Inlet temperature	323 K, 333 K and 343 K
Operation pressure	1 atm
Anode fuel	H_2 (76.5%) and H_2O (23.5%)
Cathode fuel	O_2 (21.5%), N_2 (77.2%) and H_2O (2.1%)
Relative humidity of the anode	100%

70/30% H_2/H_2O, while the cathode is fed with saturated oxygen with a mass fraction of 21/79% O_2/N_2. The N_2 gas serves as a diluent and is assumed to be inert.

In general, the straight gas flow channels used in a conventional PEMFC are designed to maximize the area of the catalyst surface exposed to the reactant gases and to provide a route for the liquid byproduct of the catalytic reaction to exit the fuel cell. In the current PEMFC with wave-like anode and cathode channels, the reactant gases experience a mixed convection effect, i.e. natural convection as a result of the elevated temperature in the gas flow channel [16,17] and forced convection as a result of the wave-like profile of the channel walls. Consequently, the wave-like gas flow channels not only maximize the reaction area and allow the water byproduct to drain from the fuel cell, but also enhance the gas velocity in the vertical direction and therefore increase the transfer of the reactant gases to the catalyst layer.

In performing the simulations, the following assumptions are made:

1. The axial velocity and temperature of the reactant gases are uniformly distributed at the inlets to both gas flow channels.
2. The reactant gases are incompressible and enter the gas flow channel in a direction normal to that of the channel cross-section. The gas flow in both channels is laminar and has a Reynolds number of less than 200.
3. The GDLs, catalyst layers and membrane are isotropic and homogeneous, and have a high permeability and a uniform porosity.
4. The electrochemical reaction is governed by the Butler–Volmer kinetic equation.
5. The water byproduct of the electrochemical reaction is in a vapor state.
6. The membrane is impervious to the reactant gases.
7. The fuel cell geometry is periodic in the x-axis direction.

Note that for computational efficiency, the model is divided into seven separate layers, namely the upper wave-like channel, the anode GDL, the anode catalyst layer (CL), the membrane, the cathode CL, the cathode GDL and the lower wave-like channel. In general, the heat and mass transfer characteristics of PEMFC gas flow channels can be modeled using conventional mass conservation, Navier–Stokes, and energy and species conservation equations. The basic 3D gas transport equations for a general PEMFC can be expressed as follows:

- Continuity equation:

$$\frac{\partial u}{\partial x} + \frac{\partial v}{\partial y} + \frac{\partial w}{\partial z} = 0. \tag{1}$$

- Momentum equation:

$$\varepsilon_{\text{eff}} \left(u\frac{\partial u}{\partial x} + v\frac{\partial u}{\partial y} + w\frac{\partial u}{\partial z} \right) = -\frac{\varepsilon_{\text{eff}}}{\rho}\frac{\partial P}{\partial x} + \upsilon\varepsilon_{\text{eff}} \left(\frac{\partial^2 u}{\partial x^2} + \frac{\partial^2 u}{\partial y^2} + \frac{\partial^2 u}{\partial z^2} \right) + S_u. \tag{2}$$

$$\varepsilon_{\text{eff}} \left(u\frac{\partial v}{\partial x} + v\frac{\partial v}{\partial y} + w\frac{\partial v}{\partial z} \right) = -\frac{\varepsilon_{\text{eff}}}{\rho}\frac{\partial P}{\partial y} + \upsilon\varepsilon_{\text{eff}} \left(\frac{\partial^2 v}{\partial x^2} + \frac{\partial^2 v}{\partial y^2} + \frac{\partial^2 v}{\partial z^2} \right) + S_v. \tag{3}$$

$$\varepsilon_{\text{eff}} \left(u\frac{\partial w}{\partial x} + v\frac{\partial w}{\partial y} + w\frac{\partial w}{\partial z} \right) = -\frac{\varepsilon_{\text{eff}}}{\rho}\frac{\partial P}{\partial z} + \upsilon\varepsilon_{\text{eff}} \left(\frac{\partial^2 w}{\partial x^2} + \frac{\partial^2 w}{\partial y^2} + \frac{\partial^2 w}{\partial z^2} \right) + S_{\text{w}}. \tag{4}$$

- Energy equation:

$$\varepsilon_{\text{eff}} C_p \left(u\frac{\partial T}{\partial x} + v\frac{\partial T}{\partial y} + w\frac{\partial T}{\partial z} \right) = \frac{k\varepsilon_{\text{eff}}}{\rho} \left(\frac{\partial^2 T}{\partial x^2} + \frac{\partial^2 T}{\partial y^2} + \frac{\partial^2 T}{\partial z^2} \right) + S_{\text{e}}. \tag{5}$$

- Species conservation equation:

$$\varepsilon_{\text{eff}} \left(u\frac{\partial C_k}{\partial x} + v\frac{\partial C_k}{\partial y} + w\frac{\partial C_k}{\partial z} \right) = D_{k,\text{eff}} \left(\frac{\partial^2 C_k}{\partial x^2} + \frac{\partial^2 C_k}{\partial y^2} + \frac{\partial^2 C_k}{\partial z^2} \right) + S_{\text{c}}. \tag{6}$$

- Charge conservation equation:

$$\varepsilon_{\text{eff}} \left(u\frac{\partial \phi_{\text{e}}}{\partial x} + v\frac{\partial \phi_{\text{e}}}{\partial y} + w\frac{\partial \phi_{\text{e}}}{\partial z} \right) = -S_\phi. \tag{7}$$

The analytical formulae for the source terms S_u, S_v, S_{w}, S_{e}, S_{c} and S_ϕ in Eqs. (2)–(7) are derived in Table 2. Note that in these formulae, the parameters ε_{eff}, C_{F}, k_{p} and Z_{f} denote the effective porosity, the quadratic drag factor, the permeability and the valence of the species, respectively. Furthermore, $D_{k,\text{eff}} = D_k \varepsilon^{\tau_i}$ represents the effective diffusion coefficient of

Table 2
Analytical formulae for source terms in governing equations (Eqs. (2)–(7))

Source terms	Flow channel	Gas diffusion layer	Catalyst layer	Membrane
S_u	0	$-\frac{\upsilon\varepsilon^2}{k_p}u-\frac{\varepsilon^3_{\text{eff}}C_F\rho u}{\sqrt{k_p}}\sqrt{u^2+v^2+w^2}$	$-\frac{\upsilon\varepsilon^2}{k_p}u-\frac{\varepsilon^3_{\text{eff}}C_F\rho u}{\sqrt{k_p}}\sqrt{u^2+v^2+w^2}$	$-\frac{\upsilon\varepsilon^2}{k_p}u-\frac{\varepsilon^2_{\text{eff}}C_F\rho u}{\sqrt{k_p}}\sqrt{u^2+v^2+w^2}+\frac{k_p}{\upsilon}Z_fC_H+F\cdot\nabla\phi\frac{\partial u}{\partial x}$
S_v	0	$-\frac{\upsilon\varepsilon^2}{k_p}v-\frac{\varepsilon^3_{\text{eff}}C_F\rho v}{\sqrt{k_p}}\sqrt{u^2+v^2+w^2}$	$-\frac{\upsilon\varepsilon^2}{k_p}v-\frac{\varepsilon^3_{\text{eff}}C_F\rho v}{\sqrt{k_p}}\sqrt{u^2+v^2+w^2}$	$-\frac{\upsilon\varepsilon^2}{k_p}v-\frac{\varepsilon^2_{\text{eff}}C_F\rho v}{\sqrt{k_p}}\sqrt{u^2+v^2+w^2}+\frac{k_p}{\upsilon}Z_fC_H+F\cdot\nabla\phi\frac{\partial v}{\partial x}$
S_w	0	$-\frac{\upsilon\varepsilon^2}{k_p}w-\frac{\varepsilon^3_{\text{eff}}C_F\rho w}{\sqrt{k_p}}\sqrt{u^2+v^2+w^2}$	$-\frac{\upsilon\varepsilon^2}{k_p}w-\frac{\varepsilon^3_{\text{eff}}C_F\rho w}{\sqrt{k_p}}\sqrt{u^2+v^2+w^2}$	$-\frac{\upsilon\varepsilon^2}{k_p}w-\frac{\varepsilon^2_{\text{eff}}C_F\rho w}{\sqrt{k_p}}\sqrt{u^2+v^2+w^2}+\frac{k_p}{\upsilon}Z_fC_H+F\cdot\nabla\phi\frac{\partial w}{\partial x}$
S_e	0	$\rho\frac{i^2_e}{k^{\text{eff}}_s}$	$\rho j\left[\lvert\eta_{\text{act}}\rvert-\frac{T\Delta S}{nF}\right]+\rho\left(\frac{i^2_m}{k^{\text{eff}}_m}+\frac{i^2_e}{k^{\text{eff}}_s}\right)$	$\rho\frac{i^2_m}{k_m}$
S_c	–	0	$H_2:-\frac{j_a}{2FC_a}$, $O_2:-\frac{j_c}{4FC_c}$, $H_2O:\frac{j_c}{2FC_c}$	$\frac{Z_f}{RT}D_{k,\text{eff},H^+}\cdot C_{H^+}\left(\frac{\partial^2\phi}{\partial x^2}+\frac{\partial^2\phi}{\partial y^2}+\frac{\partial^2\phi}{\partial z^2}\right)$
S_ϕ	–	0	j	0

the kth component of the reactant fuel [18–20]. In the PEMFC, the generation/consumption of the chemical species and the charge transfer take place only in the catalyst layer. Therefore, the source terms in Eqs. (6) and (7) can be implemented in accordance with the principles of electrochemical kinetics, i.e.

$$S_{H_2} = -\frac{j_{\text{anode}}}{2F}, \tag{8}$$

$$S_{O_2} = -\frac{j_{\text{cathode}}}{4F}, \tag{9}$$

$$S_{H_2O} = -\frac{j_{\text{cathode}}}{2F}, \tag{10}$$

where j denotes the transfer current density and is derived from the following Butler–Volmer kinetics expressions:

$$j_a = j_{a,\text{ref}}\left(\frac{C_{H_2}}{C_{H_{2,\text{ref}}}}\right)^{1/2}\left[\exp\left(\frac{\alpha_a F}{RT}\eta_{\text{act}}\right) - \exp\left(-\frac{\alpha_c}{RT}F\eta_{\text{act}}\right)\right], \tag{11}$$

$$j_c = -j_{a,\text{ref}}\left(\frac{C_{O_2}}{C_{O_{2,\text{ref}}}}\right)\left[\exp\left(\frac{\alpha_a F}{RT}\eta_{\text{act}}\right) - \exp\left(-\frac{\alpha_c}{RT}F\eta_{\text{act}}\right)\right], \tag{12}$$

where η_{act} is the surface over potential and is defined as

$$\eta_{\text{act}} = \varphi_{a,c} - \varphi_m - V_{oc}, \tag{13}$$

in which $\varphi_{a,c}$ and φ_m denote the potentials of the carbon and membrane phases in the catalyst layer, respectively, and V_{oc} is the reference open-circuit potential of the electrode.

The phase potential equation for the potential and current profile is given by [21]:

$$\frac{\partial}{\partial x}\left(\sigma_m\frac{\partial\Phi}{\partial x}\right)+\frac{\partial}{\partial y}\left(\sigma_m\frac{\partial\Phi}{\partial y}\right)=S_j, \tag{14}$$

where Φ is the phase potential function, and σ_m is the membrane conductivity and is expressed as [22]:

$$\sigma_m(T)=\sigma_m^{\text{ref}}\exp\left[1268\left(\frac{1}{303}-\frac{1}{T}\right)\right], \tag{15}$$

where σ_m^{ref} is the reference conductivity of the membrane and is given by

$$\sigma_m^{\text{ref}} = 0.005139\lambda - 0.00326, \tag{16}$$

$$\lambda=\left\{\begin{array}{ll} 0.043+17.81a-39.85a^2+36.0a^3 & \text{for}\quad 0<a\le 1 \\ 14+1.4(a-1) & \text{for}\quad 1\le a\le 3 \end{array}\right\} \tag{17}$$

in which a is the water activity and is defined as

$$a=\frac{x_{H_2O}P}{P_{\text{sat}}}. \tag{18}$$

In Eq. (18), the saturation pressure varies with the temperature and can be determined directly from thermodynamic tables or via the following empirical expression [23]:

$$P_{\text{sat}} = 10^{-2.1794+0.02953T-9.1837\times10^{-5}T^2+1.4454\times10^{-7}T^3}. \quad (19)$$

3. Boundary conditions

The governing equations for the current PEMFC model have an elliptic, partial differential form. Consequently, boundary conditions are required for all of the boundaries in the computational domain. Due to the conjugated nature of the modeling problem, the gas flow channel surfaces are included within the numerical solution domain and are treated as a fluid with particular properties.

The boundary conditions can be summarized as follows:

1. Gas flow channel inlet
   - anode inlet:

$$u = u_{\text{in}}, \quad T = T_{\text{in}}, \quad v = 0, \quad C_{H_2} = C^{\text{a}}_{H_2,\text{in}}, \quad C_{H_2O} = C^{\text{a}}_{H_2O,\text{in}}, \quad (20)$$

   - cathode inlet:

$$u = u_{\text{in}}, \quad T = T_{\text{in}}, \quad v = 0, \quad C_{O_2} = C^{\text{c}}_{O_2,\text{in}}, \quad C_{N_2} = C^{\text{c}}_{N_2,\text{in}}, \quad (21)$$

   - interface between gas flow and GDL:

$$\left.\frac{\partial u}{\partial y}\right|_{y=h_1^-} = \varepsilon_{\text{eff,GDL}} \left.\frac{\partial u}{\partial y}\right|_{y=h_1^+}, \quad \left.\frac{\partial v}{\partial y}\right|_{y=h_1^-} = \varepsilon \left.\frac{\partial v}{\partial y}\right|_{y=h_1^+}, \quad \left.\frac{\partial w}{\partial y}\right|_{y=h_1^-} = \varepsilon \left.\frac{\partial w}{\partial y}\right|_{y=h_1^+}, \quad (22)$$

   - interface between GDL and catalyst layer:

$$\varepsilon_{\text{eff,GDL}} \left.\frac{\partial u}{\partial y}\right|_{y=h_2^-} = \varepsilon \left.\frac{\partial u}{\partial y}\right|_{y=h_2^+}, \quad \varepsilon_{\text{eff,GDL}} \left.\frac{\partial v}{\partial y}\right|_{y=h_2^-} = \varepsilon_{\text{eff,CL}} \left.\frac{\partial v}{\partial y}\right|_{y=h_2^+}, \quad \varepsilon_{\text{eff,GDL}} \left.\frac{\partial w}{\partial z}\right|_{y=h_2^-} = \varepsilon_{\text{eff,CL}} \left.\frac{\partial w}{\partial z}\right|_{y=h_2^+}, \quad (23)$$

   - interface between catalyst layer and membrane:

$$u = v = w = C_k = 0. \quad (24)$$

2. Gas flow channel outlet

$$\frac{\partial u}{\partial x} = \frac{\partial v}{\partial x} = \frac{\partial w}{\partial z} = \frac{\partial T}{\partial x} = 0. \quad (25)$$

3. Upper surfaceanode gas channel:

$$u = v = w = 0, \quad (26)$$

$$T_{\text{surface}} = 298\,\text{K}. \quad (27)$$

4. Lower surfacecathode gas channel:

$$u = v = w = 0, \quad (28)$$

$$T_{\text{surface}} = 298\,\text{K}, \quad (29)$$

$$T_{\text{in}} > T_{\text{w}}. \quad (30)$$

4. Numerical method

The governing equations for the current modeling problem are coupled and nonlinear. Therefore, the equations are most conveniently solved using some form of numerical method. In the current study the continuous cell domain is discretized into several control volumes and the dependent variables are calculated at the center of each computational cell to ensure that the conservation properties of the physical quantities are maintained. The solution procedure is conducted using general purpose CFD software with the SIMPLEC (semi-implicit method for pressure-linked equations consistent) algorithm-based solver [24]. The solution procedure commences by solving the velocity fields in the momentum equation. A pressure correction process is then applied to take account of mass imbalance effects. Finally, the concentration equation and the potential equations are solved. The simulations assume that the inlet section of the channel is fully developed hydro-dynamically, and hence a fully developed velocity profile for rectangular ducts is imposed. Additionally, a forced convection regime [25,26] is imposed within the computational domain and the Navier–Stokes equations are solved under the assumption of laminar flow. Before performing the simulations, a parametric study was conducted to identify a suitable 3D grid mesh capable of generating accurate representations of the temperature and velocity gradients near the walls in order to obtain detailed insights into the electrochemical reaction and mass transport phenomena in the PEMFC. The results suggested the use of 181 nodes in the x-direction, 49 in the y-direction, and 11 in the z-direction. A grid dependency test was performed to confirm that the resulting numerical solution was independent of the grid density. In the subsequent simulations, the iterative computations were terminated once the value of the residues fell to less than 10^{-6}. The computations were performed using a PC with a 3.2 GHz Intel Pentium 4 CPU, 1 GB DDR RAM and the Windows XP operating system.

5. Results and discussion

Fig. 2(a) and (b) illustrates the distribution of the vertical component of the flow velocity in the straight gas flow channel and the wave-like gas flow channel, respectively, under operating conditions of: (1) a cell potential of 0.6 V, (2) a cathode inlet velocity of $0.1\,\text{m}\,\text{s}^{-1}$ and (3) an anode inlet velocity of $0.05\,\text{m}\,\text{s}^{-1}$. Fig. 3 illustrates the distribution of the axial flow velocity component under the same conditions. Comparing Fig. 2(a) and (b), it is clear that the periodic wave-like structure of the gas flow channel yields a significant increase in the vertical velocity component of the gas flow. The increased supply of reactant gases to the catalyst layer enhances the efficiency of the

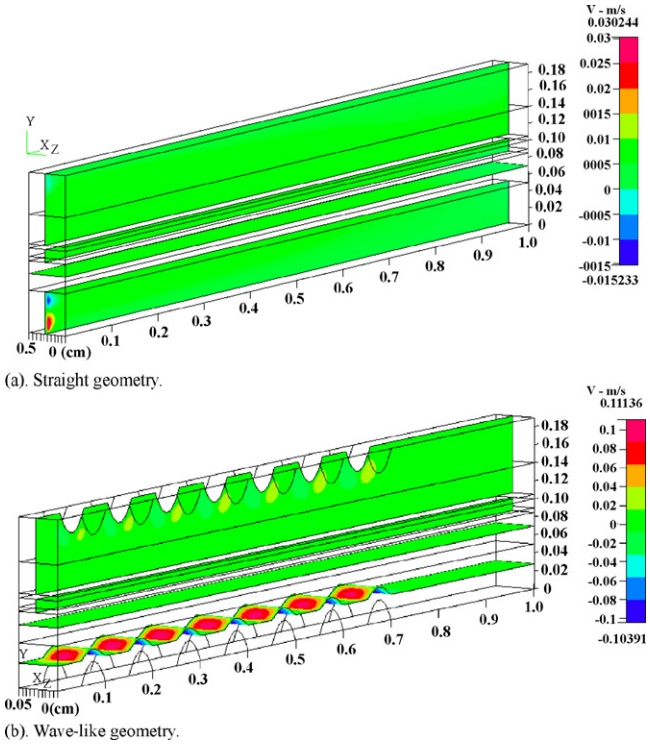

Fig. 2. Velocity field in *y*-direction of gas flow channels.

catalytic reaction and therefore improves the performance of the PEMFC. Meanwhile, comparing Fig. 3(a) and (b), it can be seen that the wave-like surface introduces a nozzle-type effect which accelerates the flow in the axial direction in the constricted region of the channel immediately above each wave feature. However,

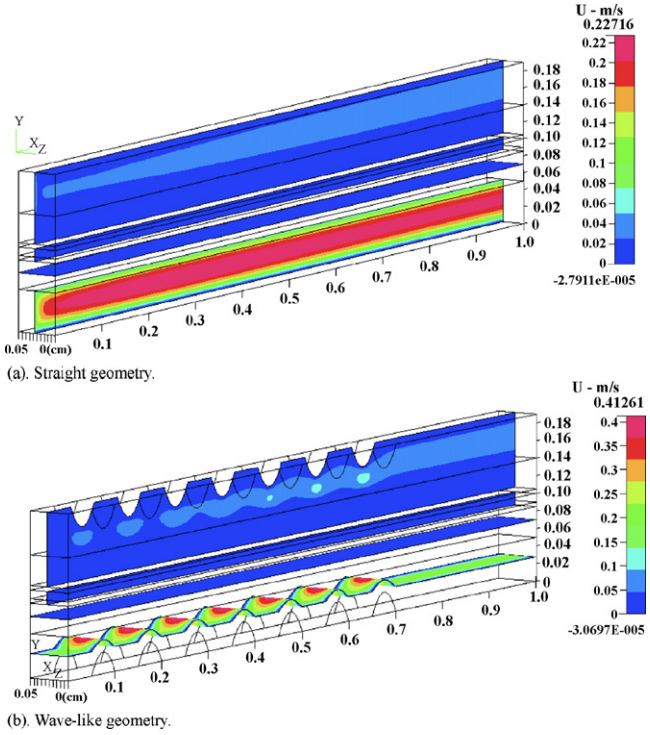

Fig. 3. Velocity field in *x*-direction of gas flow channels.

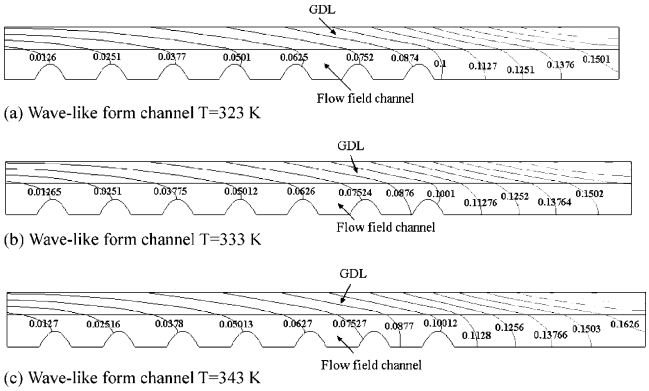

Fig. 4. Liquid water saturation field in cathode gas channel and diffusion layer at cell voltage of 0.6 V and inlet temperatures of (a) 323 K, (b) 333 K and (c) 343 K.

Fig. 3(b) also shows that the axial velocity of the reactant gases reduces in the trough regions of the wavy surface. This has the effect of trapping the fuel, thereby increasing its supply to the catalyst layer. Figs. 2 and 3 both show that a strong convective force is induced along the reaction surface of the wave-like gas flow channel. This not only increases the supply of the reactant gases to the catalyst layers, but also improves the flow of the reaction byproduct out of the PEMFC and therefore reduces the membrane drowning effect. As a result, the performance of the fuel cell is significantly improved, particularly at higher current densities.

The liquid water saturation field in the gas flow channel and the GDL on the cathode side of the PEMFC at inlet cell temperatures of 323 K, 333 K and 343 K, respectively are as Fig. 4(a)–(c). Comparing the three figures, it is observed that the level of liquid water saturation increases slightly with an increasing operating temperature. Furthermore, in every case, it can be seen that the liquid water saturation increases along the length of the channel. As a result, liquid water is formed at the interface between the membrane and the cathode catalyst layer in the outlet region of the channel. Consequently, the liquid water saturation level in the catalyst layer is higher than that in the GDL. Liquid water is transported from the catalyst layer towards the GDL by capillary action. When the liquid water reaches the interface between the GDL and the flow channel, it is transported toward the channel outlet by the drag force induced by the convective flow of the gas.

Fig. 5 presents the variation of the oxygen concentration along the channel in both the wave-like and straight gas flow channels at a cell voltage of 0.6 V and an inlet temperature of 323 K. It can be seen that the oxygen mole fraction decreases along the flow direction as a result of absorption in the catalyst layer. Furthermore, the results confirm that a greater amount of oxygen is consumed in the wave-like channel due to the forced convection effect.

Fig. 6(a)–(c) illustrates the temperature contours within the wave-like gas flow channel for inlet temperatures of 323 K, 333 K and 343 K, respectively. The results reveal that irrespective of the inlet temperature, a relatively uniform temperature distribution is obtained within the channel. Hence,

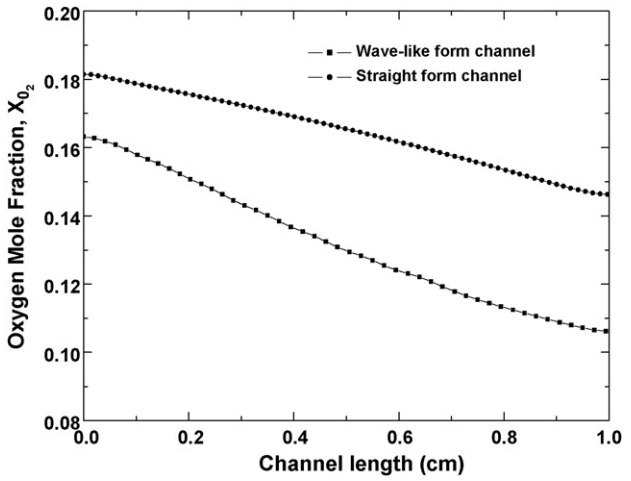

Fig. 5. Variation of oxygen mole fraction in cathode catalyst layer at cell voltage of 0.6 V.

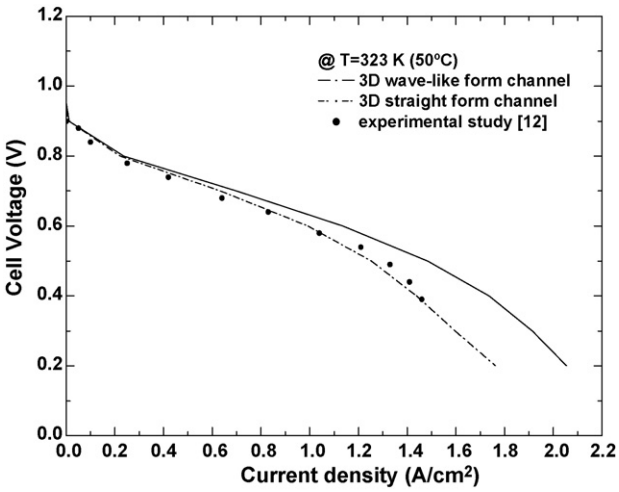

Fig. 7. Comparison of numerical predictions and experimental results [12] for variation of cell voltage with current density.

it can be inferred that the wave-like surface is instrumental in improving the heat transfer within the channel. In general, the enhanced convective heat transfer performance may be the result of the increased flow interruption caused by the wave-like obstacles in the channel, a reduction in the thermal boundary layer in the region of the channel between neighboring waves, or an increased velocity gradient near the GDL boundary.

In this study, the validity of the numerical model was verified by comparing the predicted results for the polarization characteristics of the PEMFC with the experimental data presented by Wang et al. [12]. Fig. 7 illustrates the variation of the cell voltage with the current density for both the wave-like channel and the straight channel. Note that the anode and cathode channels both have an inlet temperature of 323 K. It is clear that a good agreement exists between the numerical results for the straight gas flow channel and the experimental data, and hence the validity of the computational model is confirmed.

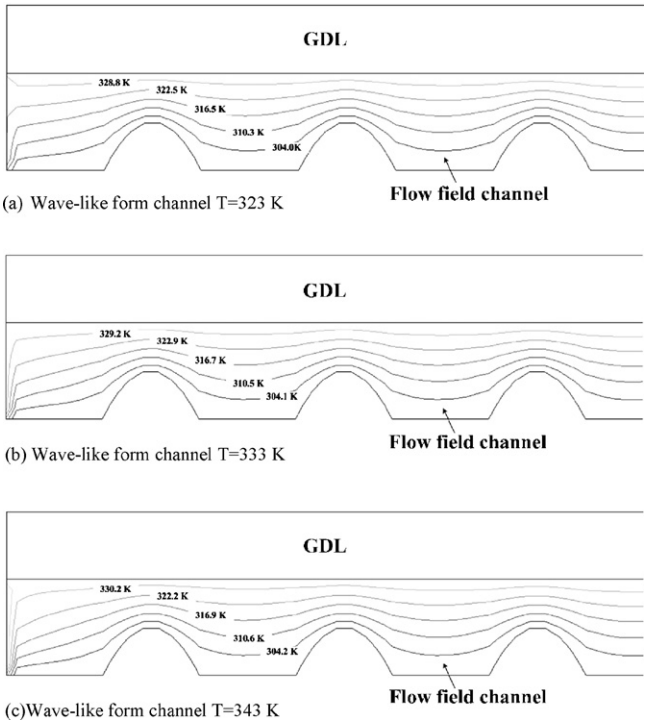

Fig. 6. Temperature contours in gas flow channel at cell voltage of 0.6 V and inlet temperatures of (a) 323 K, (b) 333 K and (c) 343 K.

Fig. 8 compares the polarization curves of the wave-like channel and the straight channel at inlet temperatures of 323 K, 333 K and 343 K, respectively. It is observed that a good agreement exists between the two sets of results at low to medium current densities. However, at high current densities, the wave-like channel yields an effective increase in both the cell voltage and the power density. The relatively poorer performance of the straight gas flow channel in the high current density region is most reasonably attributed to the lower velocity of the gas fuel supply to the GDL and catalyst layers. From a close inspection, it can be seen that both the cell voltage and the power density increase slightly as the fuel cell temperature increases. An improved PEMFC performance is obtained because a higher temperature results in a greater catalytic activity and a greater capacity for water removal via evaporation. In other words, increasing the temperature reduces the level of flooding within the fuel cell. Moreover, a higher cell temperature increases the membrane conductivity and mass diffusivity, and therefore reduces the mass transport resistance.

Fig. 9 illustrates the variation in the temperature distribution in the axial direction of the straight gas flow channel and the wave-like gas flow channel for inlet temperatures of 323 K, 333 K and 343 K. In general, it is observed that a reasonable agreement is observed between the two sets of results in the entrance region of the two gas flow channels. However, as the flow distance increases, the temperature distribution within the wave-like channel remains relatively uniform, while that within the straight channel falls rapidly. The relatively higher temperature within the wave-like channel enhances the membrane conductivity and accelerates the electrode kinetics. As a result, the electrical performance of the PEMFC is improved.

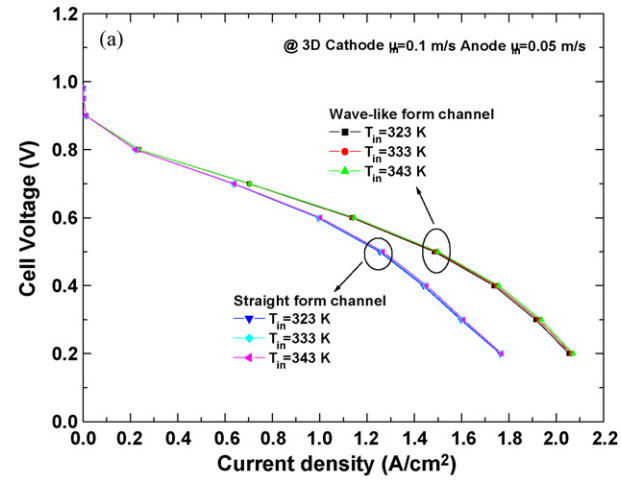

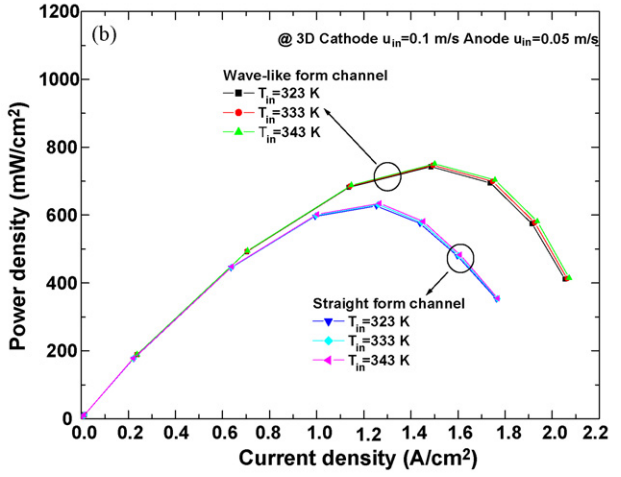

Fig. 8. Polarization curves as function of fuel cell temperature.

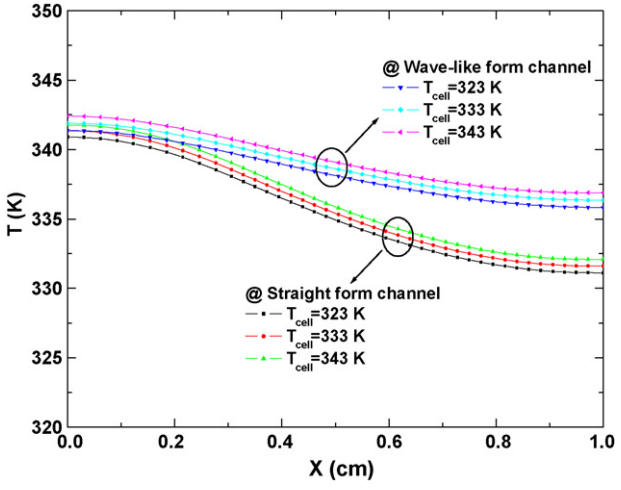

Fig. 9. Variation of temperature in GDL in inlet region of straight gas flow channel and wave-like gas flow channel for cell voltage of 0.6 V.

6. Conclusions

This study has utilized a 3D computational model to compare the fluid flow phenomena within PEMFCs containing a conventional straight gas flow channel or a novel wave-like gas flow channel. The simulations have considered inlet temperatures of 323 K, 333 K and 343 K, respectively, and have focused specifically on the influence of the forced convection effect induced in the wave-like channel on the gas flow characteristics, temperature distribution, electrochemical reaction efficiency and electrical performance of the PEMFC. In general, the results have shown that compared to a straight gas flow channel, the wave-like channel provides an improved convective heat transfer performance, a higher gas flow velocity and a more uniform temperature distribution. As a result, the efficiency of the catalytic reaction is greatly enhanced. The improved catalytic reaction results in a higher cell voltage and an improved power density, particularly at higher values of the inlet temperature and current density.

Acknowledgment

This research was supported by the National Science Council of Taiwan under contract no. NSC 96-2221-E-006-043-MY3.

References

[1] T.E. Springer, T.A. Zawodzinski, S. Gottesfeld, J. Electrochem. Soc. 136 (1991) 2334–2342.
[2] M.S. Chiang, H.S. Chu, C.K. Chen, S.R. Jian, J. Power Sources 166 (2007) 362–375.
[3] K. Haraldsson, K. Wipke, J. Power Sources 126 (2004) 88–97.
[4] R. Sousa Jr., E.R. Gonzalez, J. Power Sources 147 (2005) 32–45.
[5] D. Cheddie, N. Munroe, J. Power Sources 147 (2005) 72–84.
[6] A.Z. Weber, J. Newman, J. Electrochem. Soc. 152 (2005) A677–A688.
[7] J.K. Kuo, C.K. Chen, J. Power Sources 162 (2006) 207–214.
[8] J.K. Kuo, C.K. Chen, J. Power Sources 162 (2006) 1122–1129.
[9] J.K. Kuo, C.K. Chen, Int. J. Heat Mass Transfer 50 (2007) 4166–4179.
[10] W.M. Yan, H.C. Liu, C.Y. Soong, F. Chen, C.H. Cheng, J. Power Sources 161 (2006) 907–919.
[11] S. Dutta, S. Shimpalee, J.W. Van Zee, Int. J. Heat Mass Transfer 44 (2001) 2029–2042.
[12] L. Wang, A. Husar, T. Zhou, H. Liu, Int. J. Hydrogen Energy 28 (2003) 1263–1272.
[13] C.Y. Wang, P. Cheng, Int. J. Heat Mass Transfer 39 (1996) 3607–3618.
[14] Z.H. Wang, C.Y. Wang, K.S. Chen, J. Power Sources 94 (2001) 40–50.
[15] C.Y. Wang, Chem. Rev. 104 (2004) 4727–4766.
[16] A. Omri, S.B. Nasrallah, Numer. Heat Transfer A: Appl. 36 (6) (1999) 615–637.
[17] L. You, H. Liu, Int. J. Heat Mass Transfer 45 (2002) 2277–2287.
[18] C.I. Lee, H.S. Chu, J. Power Sources 161 (2006) 949–956.
[19] J.J. Hwang, C.H. Chao, W.Y. Ho, C.L. Chang, D.Y. Wang, J. Power Sources 157 (2006) 85–97.
[20] J.J. Hwang, P.Y. Chen, Int. J. Heat Mass Transfer 49 (2006) 2315–2327.
[21] K. Vafai, C.L. Tien, Int. J. Heat Mass Transfer 24 (1981) 152–169.
[22] T.V. Nguyen, R.E. White, J. Electrochem. Soc. 140 (1993) 2178–2186.
[23] H.C. Liu, W.M. Yan, C.Y. Soong, F. Chen, J. Power Sources 142 (2005) 125–133.
[24] C.P. Wang, H.S. Chu, J. Power Sources 159 (2006) 1025.
[25] P.L. Woodfield, K. Suzuki, K. Nakabe, Numer. Heat Transfer B: Fund. 43 (5) (2003) 403–423.
[26] D.N. Pope, G. Gogos, Numer. Heat Transfer B: Fund. 48 (3) (2005) 213–233.